



INSTITUT DE FRANCE
Académie des sciences

Comptes Rendus

Chimie

Khaled Hosni, Khaled Mahmoudi, Manel Haraketi, Salah Jellali and Ezzeddine Srasra


Mechanosynthesis, characterization, and adsorptive properties of Mg–Al-LDH and Zn–Al-LDH for olive mill wastewater treatment

Published online: 23 January 2024

Part of Special Issue: Materials and Clean Processes for Sustainable Energy and Environmental Applications

Guest editors: Mejdi Jeguirim (Université de Haute-Alsace, Institut de Sciences des Matériaux de Mulhouse, France) and Patrick Dutournié (Université de Haute-Alsace, Institut de Sciences des Matériaux de Mulhouse, France)

<https://doi.org/10.5802/crchim.265>

 This article is licensed under the
CREATIVE COMMONS ATTRIBUTION 4.0 INTERNATIONAL LICENSE.
<http://creativecommons.org/licenses/by/4.0/>



*The Comptes Rendus. Chimie are a member of the
Mersenne Center for open scientific publishing*
www.centre-mersenne.org — e-ISSN : 1878-1543

Research article

Materials and Clean Processes for Sustainable Energy and Environmental Applications

Mechanosynthesis, characterization, and adsorptive properties of Mg–Al-LDH and Zn–Al-LDH for olive mill wastewater treatment

Khaled Hosni^{✉,*},^a, Khaled Mahmoudi[✉],^a, Manel Haraketi[✉],^a, Salah Jellali[✉],^b and Ezzeddine Srasra^a

^a University of Carthage, National Center for Research in Materials Sciences (CNRSM), Laboratory of Composite Materials and Clay Minerals, Soliman, Tunisia

^b Centre for Environmental Studies and Research, Sultan Qaboos University, Al-Khoud 123, Oman

E-mails: hosnikhaled@gmail.com (K. Hosni), mahmoudikhaled1984@gmail.com (K. Mahmoudi), mharaketi@gmail.com (M. Haraketi), s.jellali@squ.edu.om (S. Jellali), srasra.ezzeddine@gmail.com (E. Srasra)

Abstract. Industrial olive oil production is of fundamental economic importance for many Mediterranean countries. However, this industry generates huge amounts of toxic olive mill wastewater (OMW), which could represent a serious threat to human health and environmental biodiversity. In the current study, calcined layered double hydroxides (LDHs) were synthesized through a mechanochemical process involving the manual grinding of magnesium or zinc- and aluminum-nitrate salts in an agate mortar, followed or not by a peptization process. The experimental results showed that non-peptized LDHs have a layered structure with relatively low crystallinity. However, the peptization process resulted in LDHs with regular particles exhibiting high crystallinity and thermal stability. These LDHs achieved a significant improvement in the quality of OMW. Indeed, after 44 h of contact time, the removed amounts of chemical oxygen demand (COD) and biological oxygen demand (BOD) were assessed at approximately 300 and 100 mg·g⁻¹, respectively. Moreover, the discoloration rate of this effluent was more than 90%. Overall, the results demonstrate the convenience of the mechanosynthesis of hydrotalcite and the high efficiency of OMW treatment, which is promising for the potential applications of calcined LDH in environmental clean-up and remediation of contaminated water.

Keywords. Layered double hydroxides, Mechanochemistry, Peptization, Olive mill wastewater treatment.

Manuscript received 4 August 2023, revised 1 October 2023, accepted 5 October 2023.

* Corresponding author.

1. Introduction

Mediterranean countries produce approximately 97% of the world's olives [1]. In the European Union, Spain, Italy, and Greece are the most important producers, whereas Tunisia is one of the largest producers in the North African region. Olive oil production is accompanied by the generation of huge amounts of solid waste (OSW) and liquid effluents. In Mediterranean countries, the olive mill wastewater (OMW) quantity was evaluated to be approximately 30 M·m³ [1]. Because of their high organic loads and toxic substance contents, such as polyphenols, the disposal of OMW into surface waters generally results in significant contamination and reduction in biodiversity [2]. Uncontrolled discharge of OMW can also be responsible for soil and groundwater pollution [3]. The phytotoxic activity of OMW is mainly attributable to their richness in monomeric phenols [4], which can seriously inhibit seed germination and plant development [5]. Therefore, it is necessary to identify the adapted technologies for the treatment of OMW prior to their discharge into the environment.

Different approaches have been developed and tested to valorize olive mill liquid and solid wastes. They include the production of energy and valuable materials using thermochemical processes such as pyrolysis and hydrothermal carbonization [6,7]. Other treatment technologies have been developed to reduce the levels of harmful substances in OMW. They include the use of chemical oxidation processes, electrocoagulation, precipitation and coagulation, sedimentation, filtration, osmosis, ion exchange, etc. [8,9]. Adsorption onto natural and synthetic materials is a promising method for the treatment of both urban and industrial effluents because it is low in cost, practical, and highly effective against a large range of pollutants [10]. For the treatment of OMW, numerous adsorbents have been employed. They primarily consist of resin [10], activated clay [11], activated carbon [12], and zeolite [13]. However, these adsorbents typically have significant prices because of both the price of the substance itself and the cost of the entire process.

The use of layered double hydroxides (LDHs) offers significant advantages over many other conventional methods. Indeed, these materials can

exhibit high adsorption capacities, higher selectivity, easier desorption, better mechanical resistance, and reusability [11]. Layered double hydroxides, also known as hydrotalcite-like compounds (HTlc) or anionic clays, are two-dimensional lamellar compounds that are formed using divalent and trivalent metal ions [12]. They have positively charged layers and charge-balancing anions located in the interlayer region [12]. The application of LDHs for wastewater treatment has attracted special attention because they are prepared from low-cost precursors and can be easily regenerated [13].

Various chemical methods have been developed for LDH synthesis. The most common method is the co-precipitation of metal salts from a mixed solution at a constant pH in the presence of anionic species that are intercalated between layers. The co-precipitation method is time-consuming and produces large amounts of waste [14,15]. Various other techniques have been proposed, including precipitation at variable pH [16], sol-gel and hydrothermal synthesis [17], structure reconstruction [18], and hydrolysis [19]. Each of these methods has its own advantages and disadvantages [20]. The search for new methods of synthesis that allow the rapid preparation of LDH has directed attention to solid-state reactions. Among these methods, mechanochemical activation appears to be a promising alternative method because of its simplicity and versatility [21]. During the mechanochemical reactions, the transformation of the solid reactants can be induced by milling or manual grinding [20]. Such reactions between solid reactants in the absence of a solvent are significant from both environmental and topochemical standpoints [20]. These solvent-free and less conventional procedures are considered viable routes for the preparation of LDHs [22]. Grinding is known to mechanically activate these reactions. The mechanical energy produced by grinding leads to the regular arrangement of the particles after proper grinding, whereas structural imperfections in the particles appear after longer grinding [23]. As a result, suitable grinding is necessary to ensure sufficient contacts and effective collisions between the reactants. The particle size and purity of hydrotalcite are important in industrial applications [24].

It is important to note that LDHs manufactured by liquid-phase approaches have been intensively used for the removal of anionic pollutants (anions

and oxyanions of the halogen elements) [25], boron species [26], oxyanions [27], etc. However, only a few studies have reviewed the application of Mg/Zn–Al-LDHs, which are synthesized by mechanochemical processes involving the manual grinding of magnesium or zinc and aluminum nitrate salts in an agate mortar followed by a peptization process [28, 29]. It is well known that the specific surface area of materials and surface defects increase as a result of mechanochemical activation processes [30]. Such changes contribute to the significant enhancement of adsorption performance [28]. Guo and Reardon [31] synthesized meixnerite by grinding MgO and Al(OH)₃ in two steps to remove fluoride ions. The results illustrated that the obtained samples could adsorb anions by an ion-exchange mechanism and also form a new phase with the anions on the surface of the adsorbent due to its outstanding surface activity.

Wang *et al.* [32] milled Mg(OH)₂ to an activated state before co-grinding it with Al(OH)₃ to create the precursor of Mg–Al-LDH. The obtained sample showed excellent adsorption capacity (1110.2 mg·g⁻¹) toward methyl orange (MO). Through surface adsorption, He *et al.* [32] successfully removed phenols from water using an Mg–Al-LDH precursor. They reported outstanding adsorption capacities of 82.6 mg·g⁻¹ for phenol and 356.4 mg·g⁻¹ for p-nitrophenol. The data demonstrated that the disorderly precursor could provide more active sites than other adsorbents, with a stable crystalline structure for the adsorption of anionic pollutants [32]. Therefore, testing this type of LDH for the treatment of real and chemically complex effluents such as OMW is of great interest. To date, no study has been conducted on the use of LDHs prepared using the solid–solid method for OMW treatment.

In this respect, the main goals of this work are as follows: (i) to synthesize Mg/Zn–Al-LDHs using a simple solid–solid method; (ii) to determine how the grinding time and the molar ratio of Mg/Al or Zn/Al affect the crystallinity of Mg/Zn–Al-LDHs; (iii) to deeply characterize these synthesized LDHs using infrared spectroscopy, thermogravimetry/differential thermal analysis (TG-DTA), BET surface area, and X-ray diffraction (XRD) analyses; and (iv) to study the adsorptive properties of Mg–Al-LDH and Zn–Al-LDH for olive mill wastewater treatment.

2. Experimental

2.1. Synthesis of Mg/Zn–Al-LDH

A series of Mg–Al-LDH and Zn–Al-LDH were synthesized by a mechanochemical approach that involves manual grinding in a mortar followed by peptization. A mixture of magnesium or zinc and aluminum nitrates was combined with NaOH pellets and manually crushed to create a paste. To remove unwanted electrolytes, the resulting paste was washed five times with distilled water. Consequently, the entire mixture was crystallized in a Teflon bottle for 24 h. To investigate the effect of the operating conditions on the formation of LDH samples, various Mg/Al and Zn/Al molar ratios, grinding times, and peptization temperatures were tested.

For comparative purposes, two samples of Mg/Zn–Al-LDH were produced using the traditional co-precipitation approach. This method involves adding, at room temperature, a solution containing Mg/Zn and Al dropwise to a solution containing Na₂CO₃ while constantly stirring [33]. A solution of NaOH (2N) was added when needed to maintain the pH of the slurry at 10.

2.2. Characterization of the synthesized materials

Various apparatuses were used to thoroughly characterize the synthesized LDHs. They include the use of an atomic absorption spectrophotometer (AAS Vario 6) for metal concentration assessment and X-ray diffraction (XRD) to determine the main present species and their degrees of crystallinity. The diffractograms were obtained using monochromated CuK radiation and a PANalytical X'Pert High-Score Plus' diffractometer. Moreover, nitrogen adsorption measurements were performed at –196 °C with an Autosorb-1 unit (Quantachrome, USA) to determine the textural properties of the samples using the multipoint Brunauer–Emmet–Teller (BET) method. Furthermore, the Fourier-transformed infrared (FT-IR) spectra of the samples were recorded by using the KBr pellet technique with a Perkin-Elmer FT-IR (model 783) instrument. Finally, the thermal decomposition of the solid samples was studied by thermogravimetric analysis (TGA) using a Shimadzu TG-50 thermobalance. In this study, 10 mg

of these samples were heated from 50 to 700 °C at a gradient of 10 °C/min under an argon flow rate of 50 mL/min.

2.3. Olive mill wastewater sampling and preparation

Fresh samples of olive mill wastewater were collected from a three-phase local automatic mill located in northwest Tunisia during the oil extraction season. The raw OMW was first centrifuged for 60 min at 6000 rpm, filtered to remove the solid contents, and stored in a refrigerator at 4 °C to reduce the effect of biodegradation. The collected OMW was physicochemically characterized by determining various parameters such as pH (HENNA instruments P211R), electrical conductivity (HENNA instruments HI2300), chemical oxygen demand (COD) by the open reflux method for a digestion time of 2 h [34], total suspended solids (TSS) by filtration through 0.45 µm filters and biological oxygen demand (BOD) by the respirometric method. Total organic carbon (TOC) was determined by using the Multi N/C 3100 system 141 (Analytik Jena GmbH, Germany).

2.4. OMW treatment and kinetic modeling

The OMW treatment experiments were carried out in 50-ml polyethylene tubes for the materials with the best properties. All experiments were performed at the same pH as that of the raw OMW sample (pH 4.7) and at room temperature (around 25 °C).

Time-dependent OMW treatment was performed using 250 mg of LDH and 20 ml of raw OMW. The mixtures were stirred at low speed (~100 rpm) for different time intervals and centrifuged. The total suspended solid (TSS), chemical oxygen demand (COD), biochemical oxygen demand (BOD), and total organic carbon (TOC) in the supernatant were then determined.

Kinetic adsorption modeling allows not only the estimation of the sorption rates but also the deduction of the main possible mechanisms involved. In the current study, the pseudo-first-order [33] and pseudo-second-order equation [35] were tested.

3. Results and discussion

3.1. Structure of synthesized LDHs

The XRD patterns of the Mg/Zn-Al-LDH prepared by the mechanochemical method at a grinding time of 15 min and without peptization for Mg/Al = 3:1 and Zn/Al = 3:1 are shown in Figures 1a and 1b, respectively.

The X-ray diffraction (XRD) patterns for the Mg-Al-LDH samples prepared by co-precipitation (for comparison) and by the mechanochemical method, respectively, shown in Figures 1a1 and 1a2, are similar. The difference between these diffractograms lies in the intensity of the reflection (00l). Both plots show sharp, symmetrical peaks at lower 2θ values, which are characteristic of lamellar hydroxide-type compounds, and also indicate a high degree of crystallinity in the samples. Reflections 003 and 006 are attributed to basal reflections, which correspond to successive stacking of brucite-like sheets. The diffraction peaks correspond to a hexagonal lattice with R-3m rhombohedral symmetry, which is commonly used to describe LDH structures. The basal reflections of (003) indicate the formation of Mg-Al-CO₃-LDH with an interlayer spacing of 0.78 nm [36]. Furthermore, the XRD pattern of LDH prepared by the mechanochemical method is consistent with that of JCPDS No. 41-1428, suggesting that this sample has a hydroxide sheet structure [37].

Concerning the Zn-Al-LDH sample, the XRD diffractogram (Figure 1b2) shows the presence of additional reflections that are different from those of LDH prepared by the conventional method (Figure 1b1), indicating a mixture of phases. The Zn-Al-LDH sample showed a layered structure, as observed from the peaks detected at 7.82, 3.89, and 2.61 Å, which correspond to planes (003), (006), and (009), respectively, for a layered hydroxide-like material [36]. This sample displays a weak and broad peak at a 2θ value of 11° compared with the sample prepared by co-precipitation under the same conditions (Zn/Al = 3). On the other hand, Zn-Al-LDH shows a structure different from that of the Mg/Al sample. The Zn-Al-LDH phase appears to be contaminated with Al(OH)₃ (JCPDS 82-2256).

The infrared spectra of the Mg-Al-LDH and Zn-Al-LDH samples are shown in Figure 2. Because of the stretching mode of the -OH structural groups in the metal hydroxide, they exhibit a broad band at

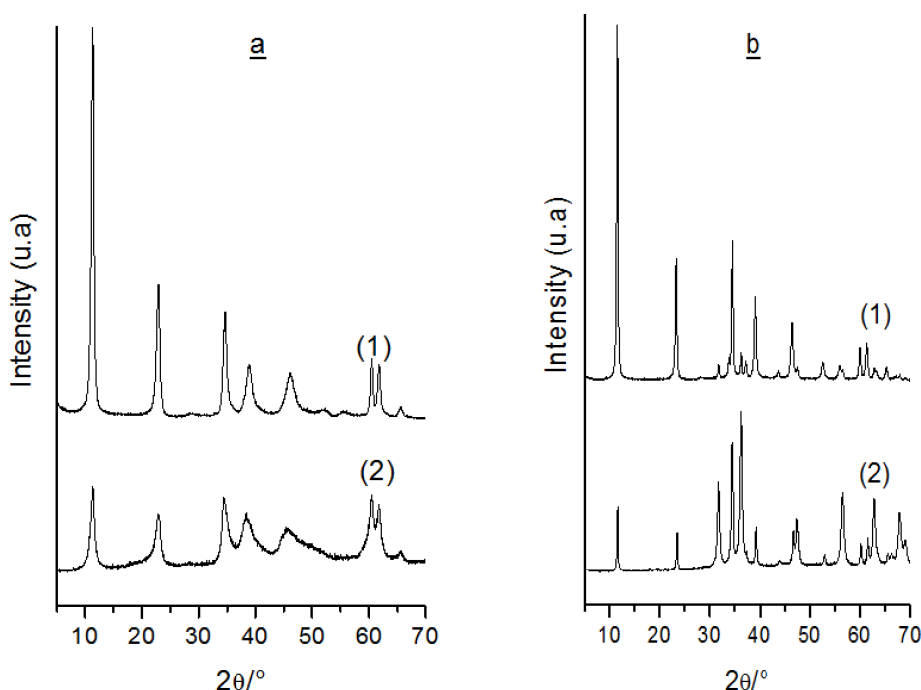


Figure 1. Powder XRD patterns: (a) Mg-Al-LDH and (b) Zn-Al-LDH prepared by (1) co-precipitation (for comparison) (2) mechanochemical method. Experimental conditions: M/Al: 3:1, grinding time = 15 min, and no peptization.

approximately 3470 cm^{-1} [38]. Both spectra (Figures 2a2 and 2b2) show a shoulder at 1638 cm^{-1} which can be attributed to the bending mode of interlayer water molecules [39]. Three characteristic bands of carbonate in hydrotalcite at $\sim 1380\text{ cm}^{-1}$ (ν_3) [40], 877 cm^{-1} (ν_2) and $\sim 1020\text{ cm}^{-1}$ (ν_1) [41] and bands around 420 and 668 cm^{-1} , which can be attributed to the Al-O and Mg-O bending modes, respectively.

The thermogravimetric analyses of the synthesized Mg-Al-LDHs and Zn-Al-LDHs are shown in Figures 3a and 3b, respectively. The shapes of the curves reflect a good degree of crystallinity for the two samples. The TGA-DTA patterns are characterized by a weight loss between 10% and 14% due to the evaporation of the interlayer-water in the temperature range of $50\text{--}250^\circ\text{C}$. For Mg-Al- CO_3 , dehydration occurs in two steps at 138°C and 216°C (Figure 3a). These steps result from the loss of adsorbed and interlayer water, followed by water coordinated to the interlayer carbonate. The interlayer carbonate was released as CO_2 at approximately 402°C (Figure 3a).

The total mass loss was estimated to be approximately 37%. For Zn-Al- CO_3 , significant mass losses at 174 , 239 , and 540°C were observed (Figure 3b). The mass losses at 174 and 240°C are accompanied by a change in the heat flow, which is the result of adsorbed surface water and interlayer water evaporation [42]. The combination of two processes, namely the dehydroxylation of the Zn-Al-LDH layers and the decomposition of the interlayer CO_3^{2-} anions, could result in the second distinct mass loss region ($350\text{--}500^\circ\text{C}$) [42].

The N_2 adsorption-desorption isotherms were of type II for all samples, which is typical of mesoporous materials (Figure 4). All materials possessed zero micropore volume. Adsorption isotherms of this type are represented by mesoporous materials with no micropores and strong interactions between the adsorbent and adsorbate molecules. This type of hysteresis loop is formed when the adsorption and desorption curves do not coincide and is physically caused by capillary condensation in the mesopores. According to the IUPAC classification [43],

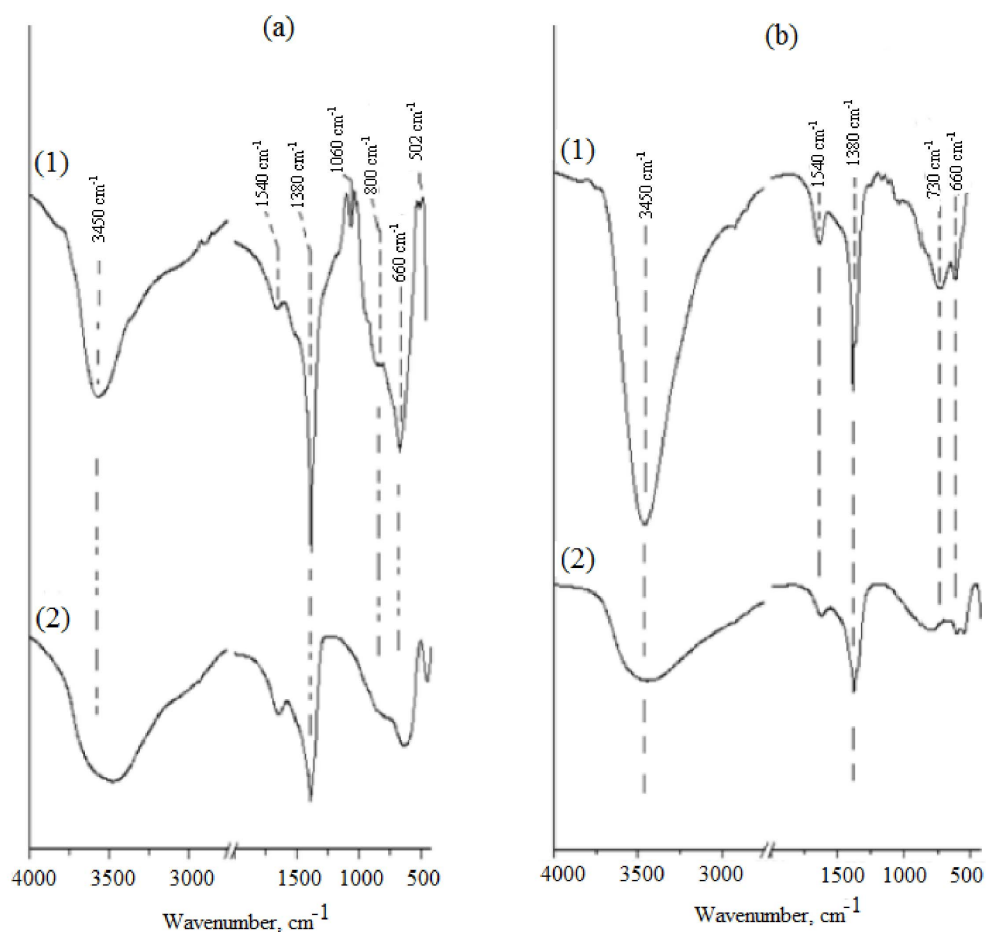


Figure 2. FTIR spectra of (a) Mg-Al-LDH and (b) Zn-Al-LDH prepared by (1) co-precipitation (for comparison) and (2) the mechanochemical method.

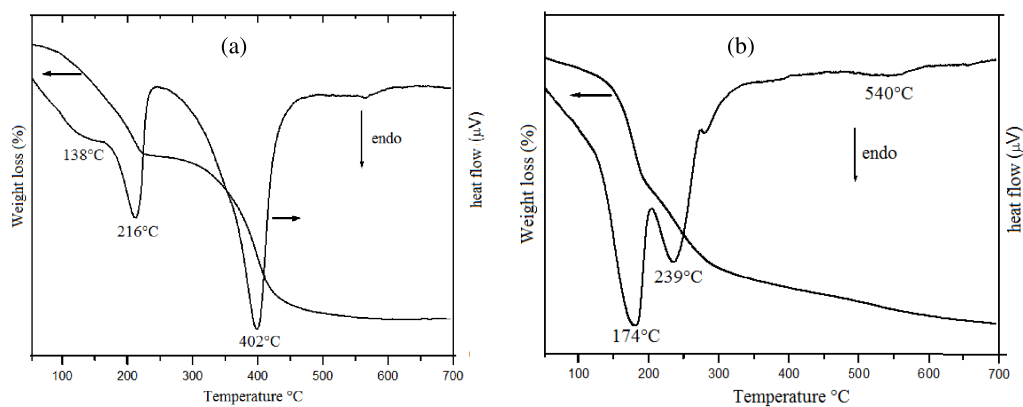


Figure 3. TG and DTA curves for (a) Mg-Al-LDH and (b) Zn-Al-LDH prepared by the mechanochemical method.

both materials display a type II isotherm with an H_3 hysteresis loop, which corresponds to solids with aggregates of plate-like particles that give rise to slit-shaped pores [44].

Specific surface areas of the Mg–Al–LDH–500 and Zn–Al–LDH–500 were determined by the single point BET method (Table 1) and were found to be 121 and 98 $\text{m}^2\cdot\text{g}^{-1}$ respectively, greater than the 77 and 65 $\text{m}^2\cdot\text{g}^{-1}$ values obtained for their precursors. It has been suggested that a porous system developed in the calcined samples during the transformation of the interlayer CO_3^{2-} to CO_2 [45].

3.2. Effect of $\text{M}^{2+}/\text{Al}^{3+}$ molar ratio on the properties of LDHs

The effect of the $\text{M}^{2+}/\text{Al}^{3+}$ ratio (R values) on the structure of Mg/Zn–Al–LDHs is shown in Figure 5. Samples prepared within the Mg/Al and Zn/Al ranges of 0.5–3 show similar patterns of natural hydrotalcite. The difference between these samples is in the intensity of the (00 l) reflection. As the Mg/Al molar ratio increased from 0.5 to 3, the intensity of the reflections increased, corresponding to an increase in crystallinity (Figure 5). This figure shows the highest crystallinity for $R = 3$. According to Bukhtiyarova *et al.* [46], a ratio of 3 produces an energetically stable LDH phase. This behavior was imputed to the fact that the more Mg^{2+} or Zn^{2+} were replaced by Al^{3+} , the stronger the bond between the layers and the intercalary anions, and therefore the LDH phase became more stable. In contrast, additional energy is introduced by the distortion of the network created by the difference in size between the two cations. In addition, a crystalline hydrotalcite phase was observed in the precipitate for Mg/Al molar ratios as low as $R = 0.5$. This can also be seen in Figure 5 that well-crystalline hydrotalcite Mg/Al compounds are formed at an Mg/Al ratio of 1:1. These samples were mixed with NaNO_3 . The LDH phase was mixed with $\text{Al}(\text{OH})_3$ in samples prepared with a Mg/Al^{3+} ratio of 0.5.

For Zn–Al–LDH (Figure 5), an LDH phase with acceptable crystallinity was obtained using only a Zn/Al molar ratio of 2. Below this ratio, the formed LDH phases were very poorly crystallized. These results are not in good agreement with those found for the synthesis of LDH by the co-precipitation method,

which showed a significant increase in the crystallinity of LDH when the $\text{M}^{2+}/\text{Al}^{3+}$ molar ratio decreased [47]. Dutta *et al.* [48] showed that increasing the Al^{3+} concentration in Zn–Al–LDH solutions causes an increase in the crystallinity of the LDH phase.

The FT-IR spectra of the synthesized samples at various Mg/Al and Zn/Al molar ratios are shown in Figure 6. These samples show spectra similar to those of natural hydrotalcite. These IR results, coupled with the above XRD results, clearly confirm that a ratio of $R = 3$ is the best molar ratio for the preparation of well-crystalline Mg–Al–LDH and Zn–Al–LDH hydrotalcite-like compounds by the mechanochemical method.

3.3. Effect of grinding time on the properties of LDHs

Grinding time and peptization temperature could also highly influence crystal growth, kinetically or thermodynamically [49]. These two key parameters control the crystallinity and particle size of the synthesized LDHs [50]. In the current work, the synthesis of Mg–Al– CO_3 and Zn–Al– CO_3 was realized by altering the grinding times while keeping the other parameters constant. Powder mixtures were prepared with Mg/Al or Zn/Al ratios of 3:1. The peptization process was performed at room temperature. The XRD patterns of the dry precipitates prepared by mechanosynthesis for grinding times of 15, 30, 60, and 90 min showed patterns similar to those of natural hydrotalcite (Figure 7). The main difference between these samples is in the intensity of the (001) reflection (Figure 7). For Mg–Al–LDH, as the grinding time increases, the intensity of the reflection increases, corresponding to an increase in crystallinity.

Similarly, Figure 7 shows the XRD patterns of Zn–Al–LDH synthesized under different grinding times. When the grinding time was increased from 15 to 60 min, the crystallinity improved, but peak heights and peak broadening were observed when the grinding time was increased to 90 min. Under shorter grinding (i.e., 30 min), the mechanical energy from shorter grinding is too weak to give rise to fully grown particles. Under longer grinding (i.e., 90 min), distortions in the plate stacking and delamination processes may account for the reduction in peak intensity as well as its widening [51].

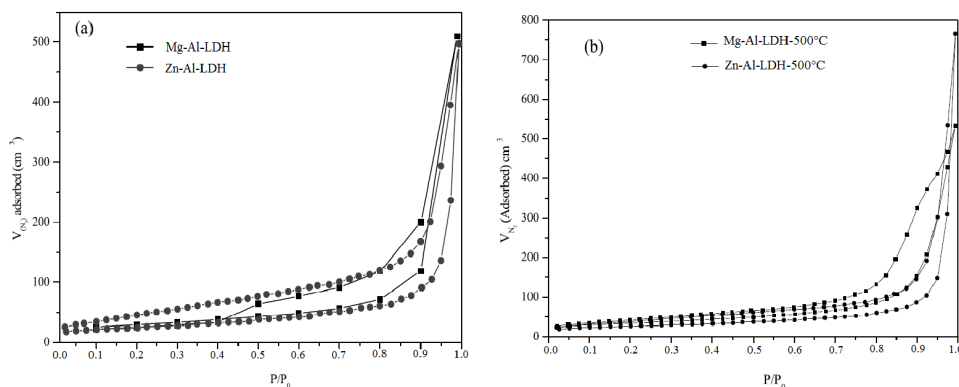


Figure 4. N₂ adsorption–desorption isotherms recorded for Mg–Al–LDH and Zn–Al–LDH: (a) before and (b) after calcination at 500 °C.

Table 1. Textural properties of Mg–Al–LDH and Zn–Al–LDH before and after calcination at 500 °C

Sample	Mg–Al–LDH		Zn–Al–LDH	
	S_{BET} (m ² ·g ^{−1})	V_{total} (cm ³ ·g ^{−1})	S_{BET} (m ² ·g ^{−1})	V_{total} (cm ³ ·g ^{−1})
Before calcination	77	0.43	66	0.79
After calcination	121	0.83	98	1.20

3.4. Effect of peptization temperature on the properties of LDHs

The peptization temperature is an important factor in the formation of all hydrotalcite-type materials via the mechanochemical route. Samples prepared within the temperature range of ambient room temperature to 150 °C show patterns similar to those of natural hydrotalcite (Figure 8). The difference between these samples is in the intensity of the (00 l) reflection. The sample of Mg–Al–LDH prepared at 120 °C shows fine and intense peaks compared with those prepared at 90 °C and 150 °C (Figure 8). The XRD patterns of the Zn–Al–LDH sample prepared at 90 °C show broad peaks, indicating poor crystallinity (Figure 8). As shown in this figure, a layered structure with high crystallinity was obtained at a peptization temperature of 120 °C, regardless of the nature of the cation. These results are in agreement with those of Zhang and Li (2013) [14], who prepared Mg–Al–LDHs, Zn–Al–LDHs, Ni–Al–LDHs, and Mg–Fe–LDH samples with high crystallinity at a peptization temperature of 100 °C. The results of the above analysis clearly indicate that Mg/Zn–Al–LDHs materials with high crystallinity and stability could be obtained af-

ter peptization. Furthermore, the peptization process probably plays a critical role in the formation of Mg/Zn–Al–LDHs with high crystallinity, and the optimum peptization temperature mainly depends on the cations used.

3.5. Textural properties

The textural properties of the LDHs prepared under different conditions are presented in Figure 9. It can be clearly concluded that the grinding time and molar ratio affect the textural properties the most. Indeed, the specific surface area of the Mg–Al–LDH samples increased by approximately 108% when the Mg–Al molar ratio increased from 0.5 to 3 and by 32% when the grinding time increased from 15 to 90 min. Moreover, the Mg–Al–LDH obtained by the mechanochemical method with an R value of 3, a peptization temperature of 25 °C, and a grinding time of 90 min has the greatest surface area (103 m²·g^{−1}), making it a potential material for anionic exchange applications. The specific surface area of the Zn–Al system increases primarily as a function of the Zn/Al molar ratio and peptization temperature (Figure 9). Indeed, S_{BET} increased by 225% when the molar ratio

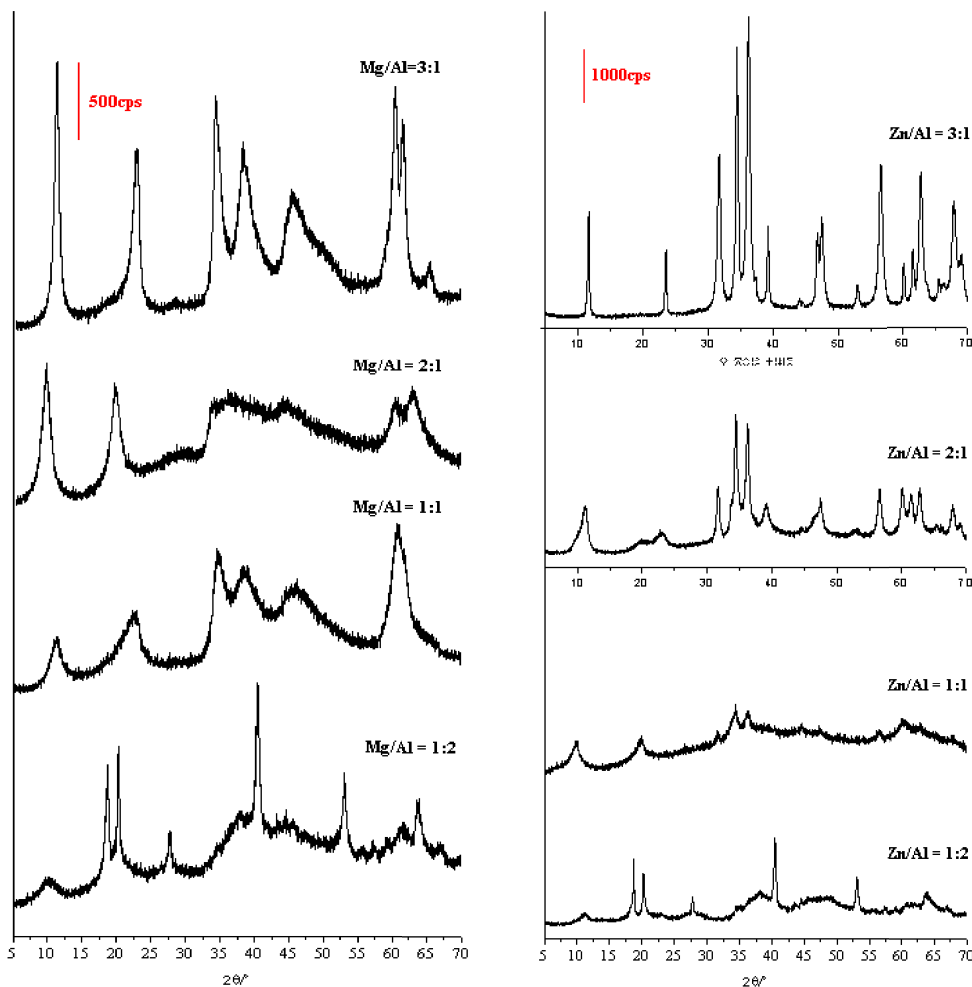


Figure 5. X-ray diffraction (XRD) patterns of LDHs prepared at a grinding time of 15 min and various Mg/Al and Zn/Al molar ratios without peptization.

increased from 0.5 to 3. On the other hand, the specific surface area reached its maximum for a grinding time of 30 min. The highest surface area was recorded for the LDH synthesized under the following conditions: Zn/Al = 3, $T = 150^\circ\text{C}$, and a grinding time of 15 min. This behavior is explained by the fact that the grinding procedure ensures homogeneity of the mixed raw materials. In addition, this process leads to the formation of primary LDH nuclei. During the heating process, the nuclei grow to form LDH of high crystallinity. The Brunauer–Emmett–Teller (BET) surface area is correlated with the presence of intercrystalline pores and the better crystallinity of the sample. On the other hand, because of the rapid nucleation in the mechanochemical process, some

Al^{3+} ions might have become overloaded on the surface sites, resulting in a higher surface charge and hence a positive surface charge density value. The correlation of surface charge density and the Mg:Al ratio with the microporous structure of LDHs was analyzed by Weir and Kydd [52]. It is likely that materials with a high surface charge density contain smaller pores, and slight changes in the layer composition may yield different BET surface areas.

3.6. Treatment of olive mill effluent

The OMW sample was characterized according to standard methods for the examination of water and

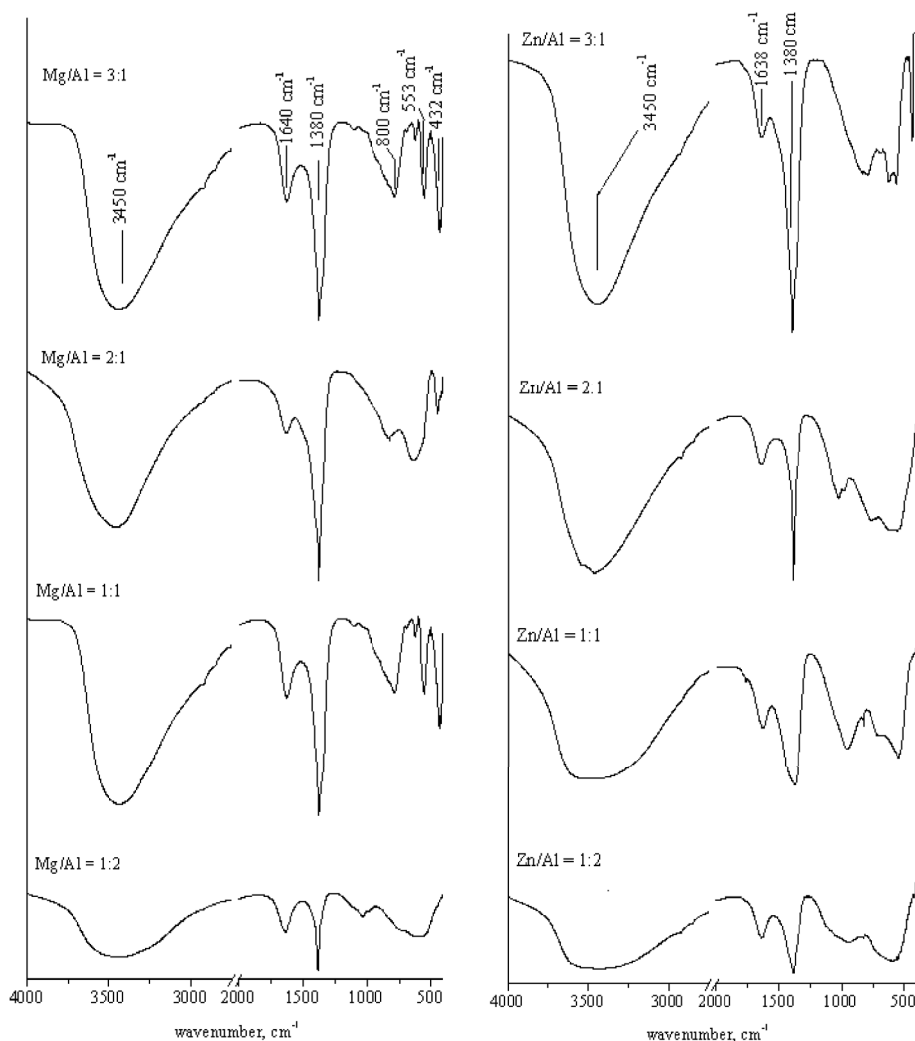


Figure 6. Infrared spectra of the dry precipitates prepared at a grinding time of 15 min, various Mg/Al and Zn/Al molar ratios, and without peptization.

wastewater [53]. Table 2 lists the main physicochemical characteristics of OMW. The pH of the OMW was acidic (4.7) because of the presence of fatty acids. This low pH value indicates that biological activities in OMW may be inhibited or very limited. The OMW electrical conductivity was determined to be $18.25 \text{ mS}\cdot\text{cm}^{-1}$, which is relatively significant and can be attributed to the presence of a high dissolved salt content. BOD_5 was equal to $25.0 \text{ g}\cdot\text{L}^{-1}$, which is comparable to the value reported by Haddad *et al.* [54]. The COD content was estimated to be $212.0 \text{ g}\cdot\text{L}^{-1}$, which is exceptionally high and is mainly due to the

presence of organic matter in both suspended and decanting materials [9]. On the other hand, OMW seems to be a real environmental problem. Some preliminary adsorption assays showed that the adsorbents were not efficient in treating the raw OMW. Therefore, the OMW was diluted twice with deionized water.

The COD, BOD, TOC, and TSS reduction kinetics were determined under the experimental conditions described in Section 2.4. The results (Figure 10a) show that the removal of COD by Zn–Al-LDH increases within the first 3 h. No significant variation

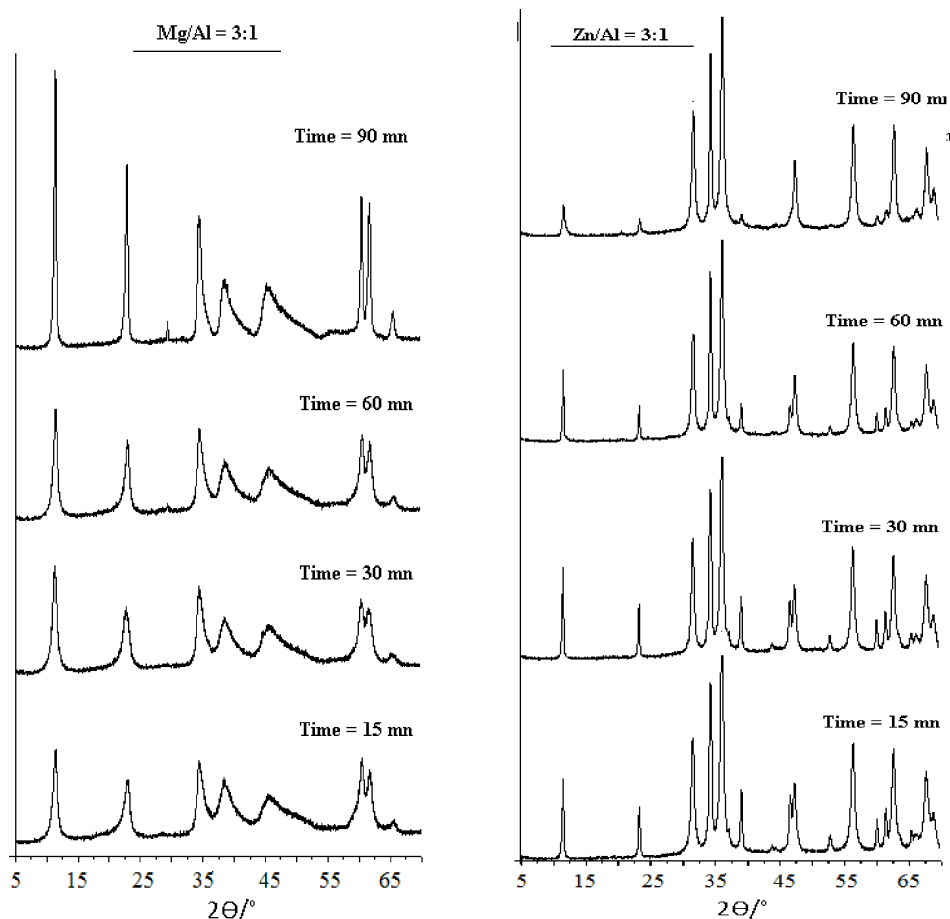


Figure 7. XRD patterns of Mg–Al-LDH and Zn–Al-LDH prepared for Mg/Al = 3 and Zn/Al = 3 at various grinding times and without peptization.

Table 2. Main physicochemical properties of the raw OMW sample

Parameters	Unit	Value
pH	-	4.7
Conductivity	mS/cm	18.25
Turbidity	NTU	11,000
Total suspended solids (TSS)	mg/L	1530
Chemical oxygen demand (COD)	g/L	212.0
Biological oxygen demand (BOD)	g/L	25.0
Total nitrogen	mg/L	0.26
Total organic carbon (TOC)	g/L	33.8

was observed after this period. For Mg–Al-LDH, the efficiency of COD removal increased with increasing

contact time, reaching a state of near equilibrium after a contact time of 44 h. When Al Bsoul *et al.* [55] treated OMW with titanium oxide nanoparticles, they observed the same behavior. These authors found that an equilibrium state could be reached after 4 h of treatment.

The maximum adsorption capacities were found to be 292 mg·g⁻¹ and 294 mg·g⁻¹ for Mg–Al-LDH and Zn–Al-LDH, respectively. These adsorbed amounts are much higher than those reported by Azzam *et al.* [56], where only 10% of the contained COD was removed. This removal process may be mainly attributed to surface complexation in the LDH structure and intercalation of the OMW organic matter into the LDH interlayer. The kinetic curves (Figures 10b, 10c, and 10d) of the removal of BOD, TOC,

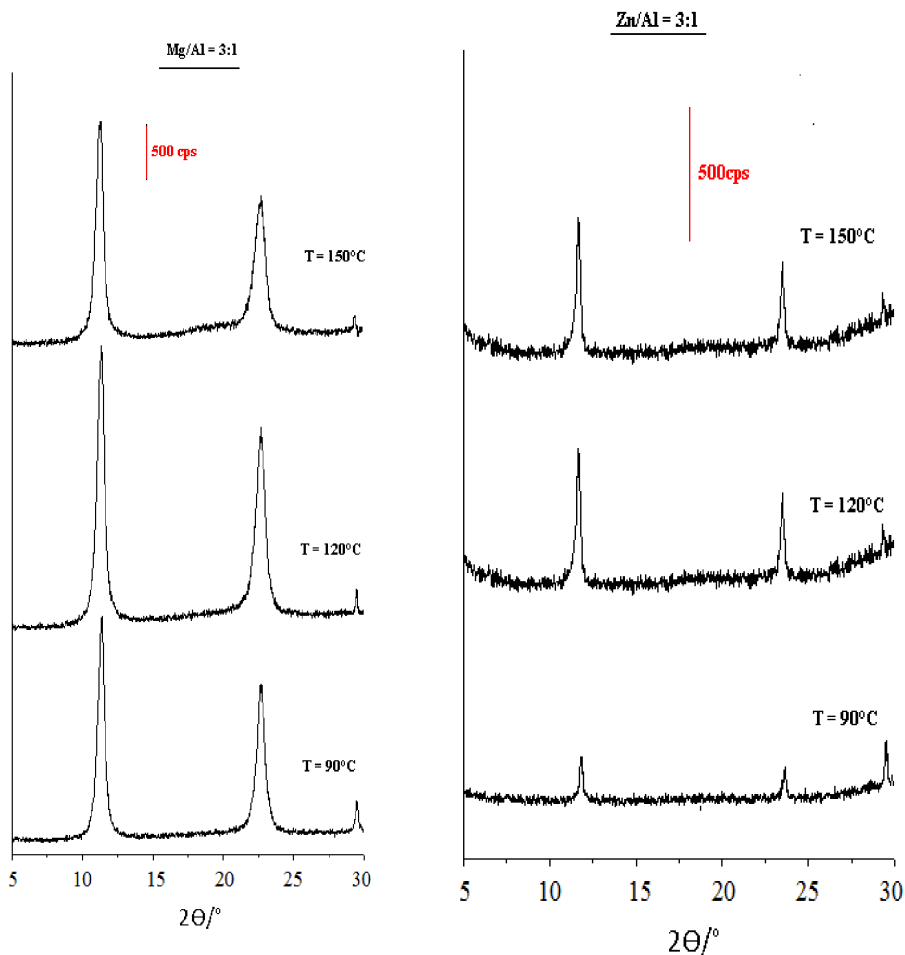


Figure 8. XRD patterns of Mg–Al-LDH and Zn–Al-LDH for Mg/Al = 3 and Zn–Al = 3 at a grinding time of 15 min and at various peptization temperatures.

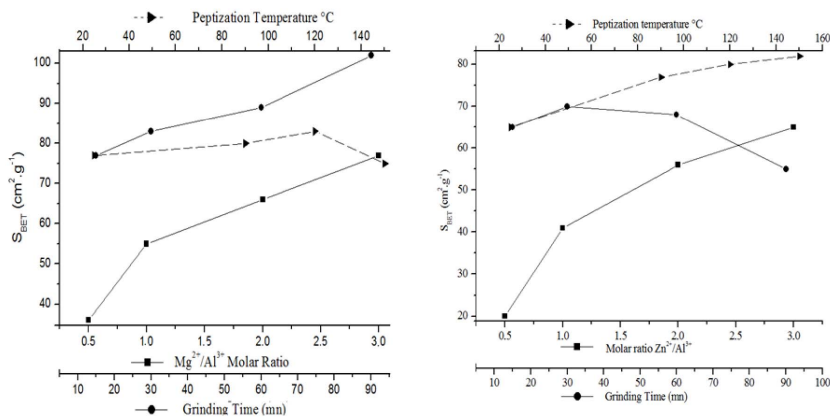


Figure 9. S_{BET} for various Mg–Al-LDH and Zn–Al-LDH samples prepared using the mechanochemical method in terms of the M/Al molar ratio, grinding time, and peptization temperature.

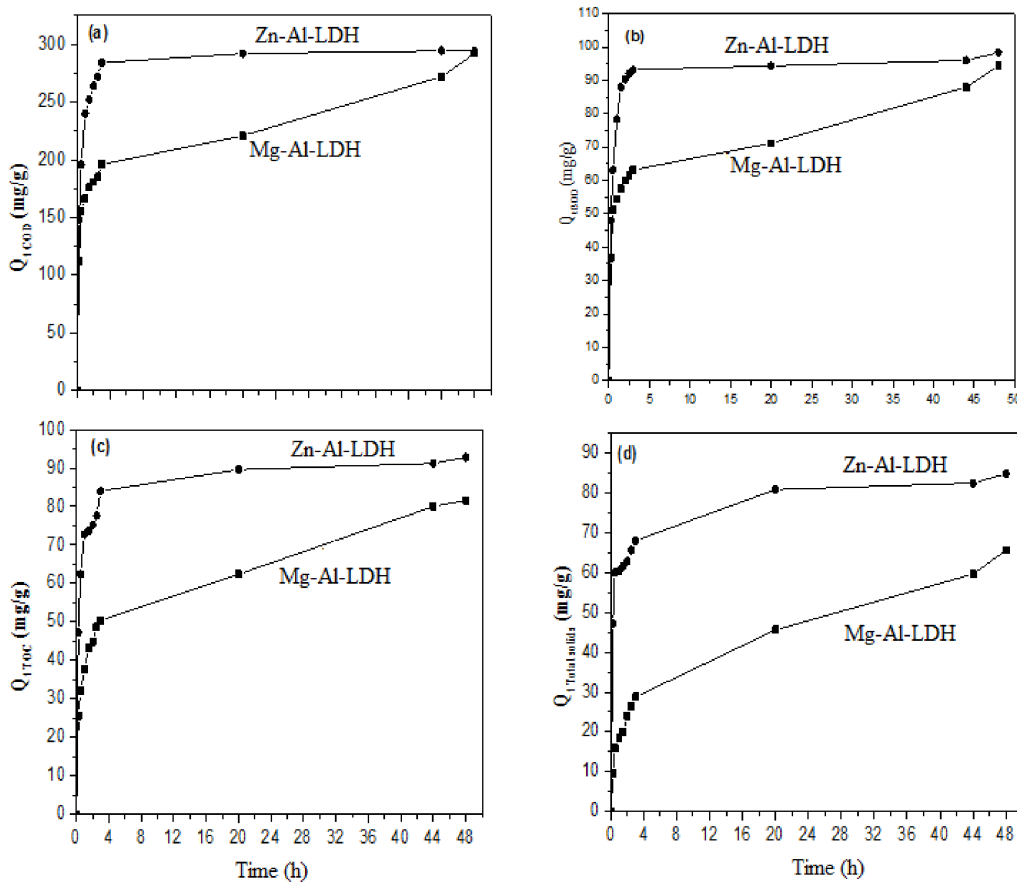


Figure 10. Effect of contact time on (a) COD, (b) BOD, (c) TOC, and (d) TSS uptake by Mg-Al-LDH and Zn-Al-LDH.

and TSS show behavior similar to that observed for COD. For instance, for Zn-Al-LDH, only a duration of 20 h was necessary to reach an equilibrium state, and the maximum TOC removed quantity was approximately $92 \text{ mg} \cdot \text{g}^{-1}$; however, a duration of 48 h was required for Mg-Al-LDHs. These results indicate that both Mg-Al-LDH and Zn-Al-LDH have relatively high efficiencies in removing COD, TOC, BOD, and TSS from the OMW.

In batch-type adsorption systems, an adsorbate monolayer typically forms on the surface of the adsorbent [57]. The rate at which an adsorbate species is transported from the exterior/outer sites to the interior sites of the adsorbent particles determines how quickly an adsorbate species is removed from an aqueous solution [58]. In addition to allowing the calculation of sorption rates, kinetic modeling produces

appropriate rate expressions representative of potential reaction mechanisms.

Although the correlation coefficient values are higher for Mg-Al-500 and Zn-Al-500, the experimental Q_{exp} values do not agree with the calculated values obtained from the linear plots (Table 3). This demonstrates that COD, BOD, TOC, and TS removal from the body and onto LDH are not first-order kinetics. When using second-order kinetics, the t/q versus t plot should be linear. There is no need to know any parameter beforehand, and Q_e and k_2 can be determined from the slope and intercept of the plot. Furthermore, this procedure is more likely to predict behavior across the entire range of uptake. The correlation coefficients for the second-order kinetic model are greater than 0.98, indicating the applicability of this kinetic equation and the

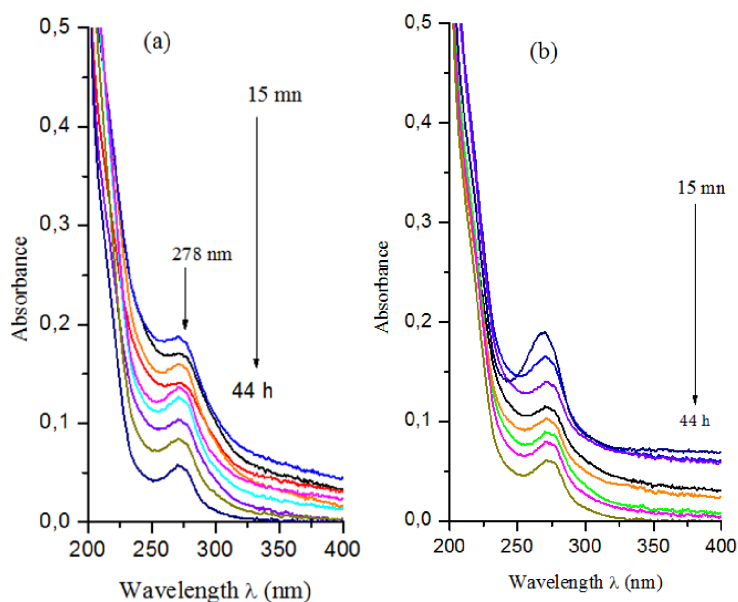


Figure 11. Visible-UV absorbance for different time periods: (a) Mg-Al-LDH and (b) Zn-Al-LDH.

Table 3. Kinetic parameters for OMW treatment with Mg-Al-LDH and Zn-Al-LDH

		Pseudo-first order			Pseudo-second order			Q_{exp}
		$Q_1, \text{mg} \cdot \text{g}^{-1}$	k_1, h^{-1}	R_1^2	$Q_2, \text{mg} \cdot \text{g}^{-1}$	k_2, h^{-1}	R_2^2	
Mg-Al-500 °C	TS	61.1	0.117	0.693	65.6	0.004	0.984	65.5
	COD	162.3	0.100	0.699	285.3	0.002	0.990	292.2
	BOD	49.2	0.087	0.737	73.5	0.013	0.990	94.1
	TOC	57.0	0.128	0.801	81.8	0.007	0.991	81.7
Zn-Al-500 °C	TS	29.8	0.115	0.765	84.2	0.022	0.999	84.6
	COD	50.5	0.135	0.907	294.0	0.014	1.000	294.2
	BOD	16.3	0.077	0.703	98.3	0.041	0.999	98.1
	TOC	25.6	0.116	0.785	92.1	0.029	0.999	92.0

second-order nature of the COD, BOD, TOC, and TS uptake processes on calcined LDH. It is worth mentioning that our materials can be considered promising materials for OMW treatment in comparison with eucalyptus sawdust [59], activated clay [60], and chitosan [61].

Coloring is considered to be an indicator of pollution from dissolved organic matter [62]. The studied OMW sample is dark in color (brown). This coloration is largely due to the presence of phenolic compounds [63], and its variation is related to the types of distribution of these compounds [64].

In addition, UV visible spectroscopy analyses (Figure 11) showed the existence of UV absorbance bands around 278 nm, which correspond to the absorption domain of polyphenols.

From Figure 11, it can be clearly seen that the treatment of OMW with Mg- and Zn-LDH significantly decreased the absorption intensity at 278 nm as the contact time increased. This peak corresponds to organic matter, particularly polyphenols. After 44 h, the absorbance measurement, or index of rejection discoloration, measured in the visible range (at 395 nm), showed that the percentage of discoloration

reached 90% for Mg–Al-LDH and 97% for Zn–Al-LDH.

4. Conclusions

This work shows that the properties of calcined Mg–Al-LDH and Zn–Al-LDH using a mechanochemical approach are dependent on various parameters, including grinding time, peptization temperature, and metal ratios. Under some experimental conditions, this rapid, simple, and inexpensive method permits the production of well-defined and homogeneous LDH particles. These materials achieve high removal efficiencies for various mineral and organic pollutants in the OMW. In the future, we intend to complete the conversion of the precursors to produce almost phase-pure LDH. This stage will be achieved through a two-step milling operation (dry and wet milling) in a mixer mill while adjusting the ball/sample ratio or the imparted mechanochemical energy. Moreover, an ecotoxicological assessment of the treated OMW will be performed.

Declaration of interests

The authors do not work for, advise, own shares in, or receive funds from any organization that could benefit from this article, and have declared no affiliations other than their research organizations.

References

- [1] E. A. N. Marks et al., *Sustainability*, 2020, **12**, article no. 6081.
- [2] C. A. Santi, S. Cortes, L. P. D'Acqui, E. Sparvoli, B. Pushparaj, *Bioresour. Technol.*, 2008, **99**, 1945–1951.
- [3] E. Bani Hani, M. Tawalbeh, A. Al-Othamni, M. El Haj Assad, *Polish J. Environ. Stud.*, 2019, **28**, 2585–2591.
- [4] A. Fiorentino et al., *J. Agric. Food Chem.*, 2003, **51**, 1005–1009.
- [5] M. J. Krogmeier, J. M. Bremner, *Biol. Fertil. Soils*, 1989, **8**, 116–122.
- [6] K. Haddad, M. Jeguirim, S. Jellali, N. Thevenin, L. Ruidavets, L. Limousy, *Sci. Total Environ.*, 2021, **752**, article no. 141713.
- [7] L. El-Bassi et al., *Sci. Total Environ.*, 2021, **755**, article no. 142531.
- [8] I. Jum'h, A. Abdelhay, H. Al-Taani, A. Telfah, M. Alnaief, S. Rosiwal, *J. Water Reuse Desalin.*, 2017, **7**, 502–510.
- [9] M. Bargaoui, S. Jellali, A. A. Azzaz, M. Jeguirim, H. Akrou, *Environ. Sci. Pollut. Res.*, 2021, **28**, 24470–24485.
- [10] K. B. Petrotos, P. E. Gkoutisidis, M. I. Kokkora, K. G. Giankidou, A. G. Tsagkarelis, *Desalin. Water Treat.*, 2013, **51**, 2021–2029.
- [11] A. De Martino et al., *Appl. Clay Sci.*, 2011, **53**, 737–744.
- [12] F. Cavani, F. Trifirò, A. Vaccari, *Catal. Today*, 1991, **11**, 173–301.
- [13] K. Hosni, E. Srasra, *J. Water Chem. Technol.*, 2011, **33**, 164–176.
- [14] X. Zhang, S. Li, *Appl. Surf. Sci.*, 2013, **274**, 158–163.
- [15] Z. P. Xu et al., *J. Am. Chem. Soc.*, 2006, **128**, 36–37.
- [16] T. Yamaoka, M. Abe, M. Tsuji, *Mater. Res. Bull.*, 1989, **24**, 1183–1199.
- [17] S. P. Paredes, G. Fetter, P. Bosch, S. Bulbulian, *J. Mater. Sci.*, 2006, **41**, 3377–3382.
- [18] T. Sato, T. Wakabayashi, M. Shimada, *Ind. Eng. Chem. Prod. Res. Dev.*, 1986, **25**, 89–92.
- [19] M. A. Ulibarri, M. J. Hernandez, J. Cornejo, C. J. Serna, *Mater. Chem. Phys.*, 1986, **14**, 569–579.
- [20] A. N. Ay, B. Zümreoglu-Karan, L. Mafra, *Z. für Anorg. und Allg. Chem.*, 2009, **635**, 1470–1475.
- [21] A. Fahami, R. Ebrahimi-Kahrizsangi, B. Nasiri-Tabrizi, *Solid State Sci.*, 2011, **13**, 135–141.
- [22] R. Chitrakar, S. Tezuka, A. Sonoda, K. Sakane, K. Ooi, T. Hirotsu, *Chem. Lett.*, 2007, **36**, 446–447.
- [23] E. Yalamac, *Ceram. Int.*, 2006, **32**, 825–832.
- [24] J. Oh, *Solid State Ionics*, 2002, **151**, 285–291.
- [25] F. L. Theiss, S. J. Couperthwaite, G. A. Ayoko, R. L. Frost, *J. Colloid Interface Sci.*, 2014, **417**, 356–368.
- [26] F. L. Theiss, G. A. Ayoko, R. L. Frost, *J. Colloid Interface Sci.*, 2013, **402**, 114–121.
- [27] K.-H. Goh, T.-T. Lim, Z. Dong, *Water Res.*, 2008, **42**, 1343–1368.
- [28] F. Zhang, N. Du, H. Li, J. Liu, W. Hou, *Solid State Sci.*, 2014, **32**, 41–47.
- [29] F. Zhang, N. Du, S. Song, W. Hou, *Mater. Chem. Phys.*, 2015, **152**, 95–103.
- [30] V. A. Baki, X. Ke, A. Heath, J. Calabria-Holley, C. Terzi, M. Sirin, *Cem. Concr. Res.*, 2022, **162**, article no. 106962.
- [31] Q. Guo, E. J. Reardon, *Appl. Clay Sci.*, 2012, **56**, 7–15.
- [32] B. Wang, J. Qu, X. Li, X. He, Q. Zhang, *J. Am. Ceram. Soc.*, 2016, **99**, 2882–2885.
- [33] S. Lagergren, *Handlingar*, 1898, **24**, 1–39, [Online]. Available: [https://www.scirp.org/\(S\(vtj3fa45qm1ean45vffcz55\)\)/reference/ReferencesPapers.aspx?ReferenceID=62289](https://www.scirp.org/(S(vtj3fa45qm1ean45vffcz55))/reference/ReferencesPapers.aspx?ReferenceID=62289).
- [34] J. Rodier, B. Legube, N. Merlet, *L'analyse de l'eau - 9ème édition - Eaux naturelles, eaux résiduaires, eau de mer*, Dunod, 2009.
- [35] Y. Ho, G. McKay, *Process Biochem.*, 1999, **34**, 451–465.
- [36] S. Miyata, *Clays Clay Miner.*, 1975, **23**, 369–375.
- [37] A. de Roy, C. Forano, K. El Malki, J.-P. Besse, *Expanded Clays and Other Microporous Solids*, Springer US, Boston, MA, 1992, 108–169 pages.
- [38] J. M. Fernández, M. A. Ulibarri, F. M. Labajos, V. Rives, *J. Mater. Chem.*, 1998, **8**, 2507–2514.
- [39] J. Theo Klopogge, R. L. Frost, *Appl. Catal. A: Gen.*, 1999, **184**, 61–71.
- [40] E. Alvarezayuso, H. Nugteren, *Water Res.*, 2005, **39**, 2535–2542.
- [41] J. T. Klopogge, D. Wharton, L. Hickey, R. L. Frost, *Am. Mineral.*, 2002, **87**, 623–629.
- [42] K. Parida, J. Das, *J. Mol. Catal. A: Chem.*, 2000, **151**, 185–192.
- [43] E. M. Seftel et al., *Microporous Mesoporous Mater.*, 2008, **113**, 296–304.
- [44] C. García-Sancho, R. Moreno-Tost, J. M. Mérida-Robles, J. Santamaría-González, A. Jiménez-López, P. M. Torres, *Catal. Today*, 2011, **167**, 84–90.
- [45] J. C. M. C. Hermosin, I. Pavlovic, M. A. Ulibarri, *Water Res.*, 1996, **30**, 171–177.

- [46] M. V. Bukhtiyarova, *J. Solid State Chem.*, 2019, **269**, 494-506.
- [47] A. Elhalil *et al.*, *J. Sci. Adv. Mater. Devices*, 2018, **3**, 188-195.
- [48] K. Dutta, S. Das, A. Pramanik, *J. Colloid Interface Sci.*, 2012, **366**, 28-36.
- [49] J. K. Lin, J. Y. Uan, *Corros. Sci.*, 2009, **51**, 1181-1188.
- [50] T. L. P. Galvão *et al.*, *J. Colloid Interface Sci.*, 2016, **468**, 86-94.
- [51] U. Mingelgrin, L. Kliger, M. Gal, S. Saltzman, B. Dagan, *Clays Clay Miner.*, 1978, **26**, 299-307.
- [52] M. R. Weir, R. A. Kydd, *Microporous Mesoporous Mater.*, 1998, **20**, 339-347.
- [53] A. E. Greenberg, L. S. Clesceri, A. D. Eaton, *Standard Methods for Examination of Water and Wastewater*, 18th ed., American Public Health Association (APHA), American Water Works Association (AWWA) and Water Pollution Control Federation (WPCF), 1992.
- [54] K. Haddad, *ACS Sustain. Chem. Eng.*, 2017, **5**, 8988-8996.
- [55] A. Al Bsoul, M. Hailat, A. Abdelhay, M. Tawalbeh, I. Jum'h, K. Bani-Melhem, *Sci. Total Environ.*, 2019, **688**, 1327-1334.
- [56] M. O. J. Azzam, S. I. Al-Gharabli, M. S. Al-Harabsheh, *Desalin. Water Treat.*, 2015, **53**, 627-636.
- [57] K. Mahmoudi, K. Hosni, N. Hamdi, E. Srasra, *Korean J. Chem. Eng.*, 2015, **32**, 274-283.
- [58] W. J. Weber, C. J. Morris, *Proceeding of 1st International Conference on Water Pollution Research*, vol. 2, Pergamon Press, Oxford, 1962, 231 pages.
- [59] E. Ouabou, A. Anouar, S. Hilali, *J. Appl. Biosci.*, 2014, **75**, 6232-6238.
- [60] K. Al-Malah, M. O. J. Azzam, N. I. Abu-Lail, *Sep. Purif. Technol.*, 2000, **20**, 225-234.
- [61] A. L. Ahmad, S. Sumathi, B. H. Hameed, *Chem. Eng. J.*, 2005, **108**, 179-185.
- [62] V. Vinciguerra, A. D'Annibale, G. D. Monache, G. G. Sermanni, *Bioresour. Technol.*, 1995, **51**, 221-226.
- [63] M. D. González, E. Moreno, J. Quevedo-Sarmiento, A. Ramos-Cormenzana, *Chemosphere*, 1990, **20**, 423-432.
- [64] M. Hamdi, A. Khadir, J.-L. Garcia, *Appl. Microbiol. Biotechnol.*, 1991, **34**, 828-831.